Design and Analysis of a Soft Prismatic Joint

by

Amelia Tepper Servi

SUBMITTED TO THE DEPARTMENT OF MECHANICAL ENGINEERING IN PARTIAL FULFILLMENT OF THE REQUIREMENTS FOR THE DEGREE OF

BACHELORS OF SCIENCE IN MECHANICAL ENGINEERING
AT THE
MASSACHUSETTS INSTITUTE OF TECHNOLOGY

JUNE 2010

Author_____
Department of Mechanical Engineering
May 10th, 2010

Certified by_____
Martin L. Culpepper
Associate Professor of Mechanical Engineering
Thesis Supervisor

Accepted by_____
John H. Lienhard V
Professor of Mechanical Engineering
Chairman, Undergraduate Thesis Committee

Design and Analysis of a Soft Prismatic Joint

by

Amelia Tepper Servi

Submitted to the Department of Mechanical Engineering
on May 10, 2010 in partial fulfillment of the
Requirements for the Degree of Bachelor of Science in
Mechanical Engineering

ABSTRACT

This thesis documents the design and analysis of a soft prismatic joint for use in soft robotics. While this joint can be utilized in any soft robot, its immediate application is for Squishbot, a soft robot developed for the DARPA Chembot challenge. For the Squishbot application, the joint must fit within a cylindrical envelope 4cm long and 1cm in diameter, compress 1.2cm axially without buckling, and be soft such that it can undergo large deformations without plastically deforming. After considering a wide range of design concepts, a screw design was chosen. This design concept was selected because it has a high axial to bending compliance ratio and does not expand radially when compressed axially. A model was developed to describe this design as a function of its design parameters. A metric was also developed to predict based on a single-cell sample whether a full-scale model would be able to fulfill the design requirements. The model was validated with respect to the parameter of blade thickness by testing 3D printed, TangoPlus cell-pairs. The results show that the model is correct to within a factor of three over blade thickness but needs further modifications to better predict trends in joint behavior. The design still needs to be tested over other parameters such as cell height. Preliminary work was also conducted on designing a locking mechanism for the joint, but more work is needed in this area. Overall, the design presented in this thesis fulfills the project's design requirements and the model that was developed describes the joint's behavior to first order.

Thesis Supervisor: Prof. Martin Culpepper
Title: Associate Professor of Mechanical Engineering

ACKNOWLEDGEMENTS

I would like to thank Prof. Martin Culpepper for his direction throughout this project and for his academic advising in general. He has been instrumental in encouraging me to pursue future work in mechanical design.

I would also like to thank Maria Telleria for guiding me during this project. She has been a great teacher and role model.

I would like to thank Nadia Cheng and Alex Slocum Jr. for answering my questions and keeping the 3D printer in working order.

Finally, I would like to thank Matt Ritter, Nimrod Gileadi, Ben Derrett, Raju Krishnamoorthy and Arathi Ramachandaram for reading this thesis and giving me valuable feedback.

This material is based upon work supported by, or in part by, the U. S. Army Research Laboratory and the U. S. Army Research Office under contract/grant number W911NF-08-C-0055.his work was supported in part by the U.S. Defense Advanced Research Projects Agency (DARPA) under the Chemical Robots Program.

Additional funding was provided by the MIT UROP office.

Table of Contents

List of Figures

List of Tables

Chapter 1: Introduction

1.1 Purpose

The purpose of this thesis is to present the design and analysis of a soft prismatic joint for use in soft robotics. By employing a screw design as shown in Figure 1, a soft prismatic joint was developed that fulfills the design requirements of Squishbot, a soft robot developed for the Chemical Robots (Chembot) program. Using the accompanying analysis, the Squishbot design can be modified to fulfill the design requirements of other robots. Introducing this soft robotic element increases the viability of soft robots, enabling future work in this field. Soft robots are more suitable for human interaction than traditional robots, and have the potential to fulfill the societal need for human compatible robots. This renders soft robotics an area of research worth pursuing.

Figure 1: Photograph of final 3D printed soft prismatic joint.

1.2 Background

Soft robotic systems are needed in situations where a rigid robot is unsuitable. These situations include applications where a robot may be in danger of damaging the environment in which it works. This is the case for medical and human service robots. Soft robots are also needed for applications where the robot itself needs to be resilient to demolition. This may be the case for military robots that need to be impervious to being squashed. In both cases, a soft robot, defined as a robot made out of a material with a low (<1 GPa) modulus of elasticity that can undergo large displacements without plastic deformation, is desired. In addition, soft robots that can squeeze through narrow openings are desired by the United States government for use in the intelligence program.

Soft robotic elements must be designed to develop these robots. This thesis focuses on the development of a soft prismatic joint for these robots: a single degree of freedom element that is capable of large linear displacements. It is also necessary to develop a model of the joint. This allows the work presented here to be applicable to other soft robots as well as other applications.

The immediate application for this joint is as an element for a robot being developed for the Chembot. The Chembot program was created to spur development of soft robots. According to their website, "The goal of the Chemical Robots...program is to create a new class of soft, flexible, meso-scale mobile objects that can identify and maneuver through openings smaller than their dimensions and perform various tasks"[1]. The Squishbot team at MIT is one of the teams working on the Chembot program. The Squishbot robot is a soft, single actuator, centimeter scale, inchworm-like robot that employs thermorheological fluids to dictate its movement [2,3]. The soft prismatic joint described in this thesis was developed to allow the robot to inch its way through narrow holes as required by the Chembot program. Figure 2 shows

a photograph of the current version of Squishbot. The soft prismatic joint developed in this thesis will replace the white, cylindrical element located in the middle of the robot.

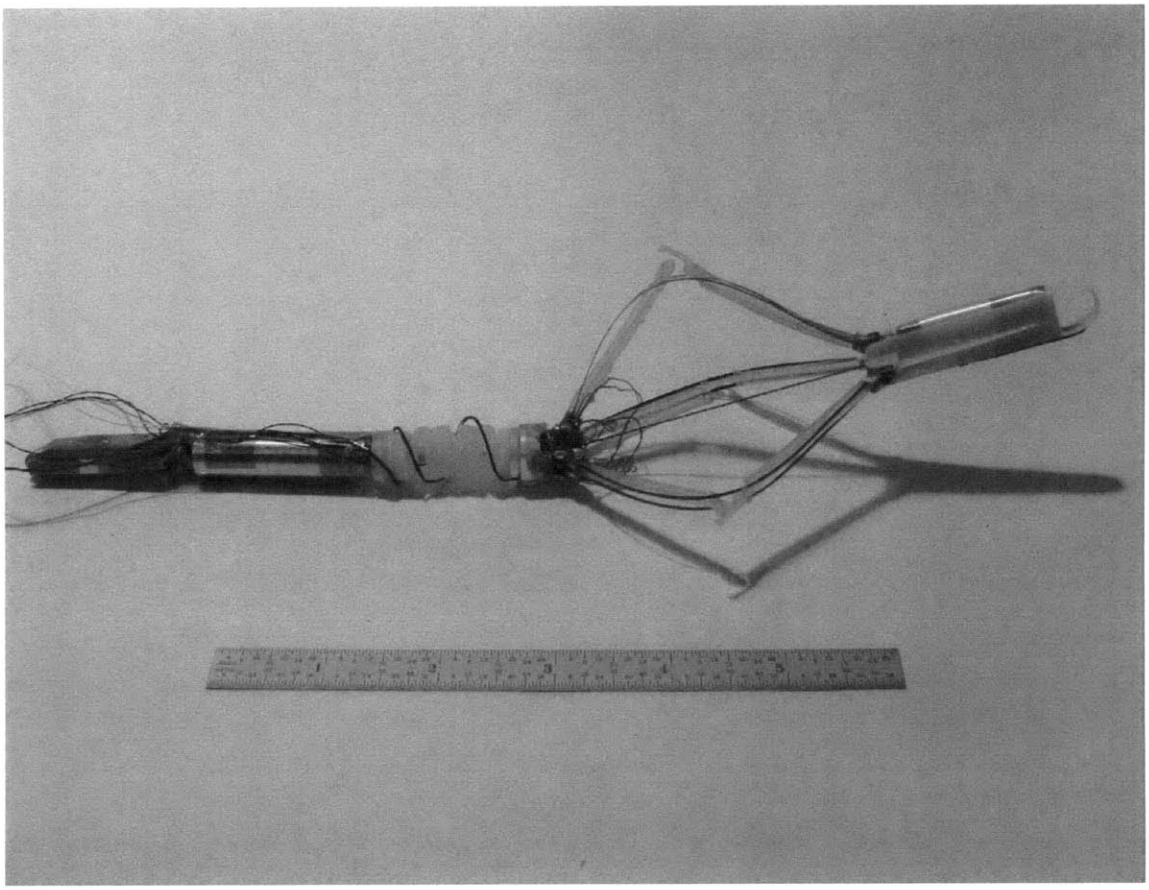

Figure 2: A photograph of Squishbot. The prismatic joint developed in this thesis will replace the white element in the middle of the robot.

Two existing technologies were considered when designing this joint. A piston exemplifies the motion desired in a prismatic joint, and it is often used as a robotic element. However, a piston is not soft. It also has sliding elements, which introduce friction forces whenever the joint deforms, thus preventing the design from being scalable to small sizes. A piston also requires assembly to manufacture and does not incorporate a restoring force making it difficult to implement in a small robot.

On the other extreme, a sponge-like structure as shown in Figure 3 is currently being used as the prismatic joint for Squishbot[4]. While the sponge-like structure is soft, requires a low actuation force, incorporates a restoring force and is assembly-free, it does not act very closely to

an ideal prismatic joint. In particular, it is prone to buckling and cannot support its own weight when cantilevered. In addition, the sponge design that is currently being used has not been modeled and so cannot be easily modified to produce the desired behavior. Thus, there is a need for the development of a new soft prismatic joint.

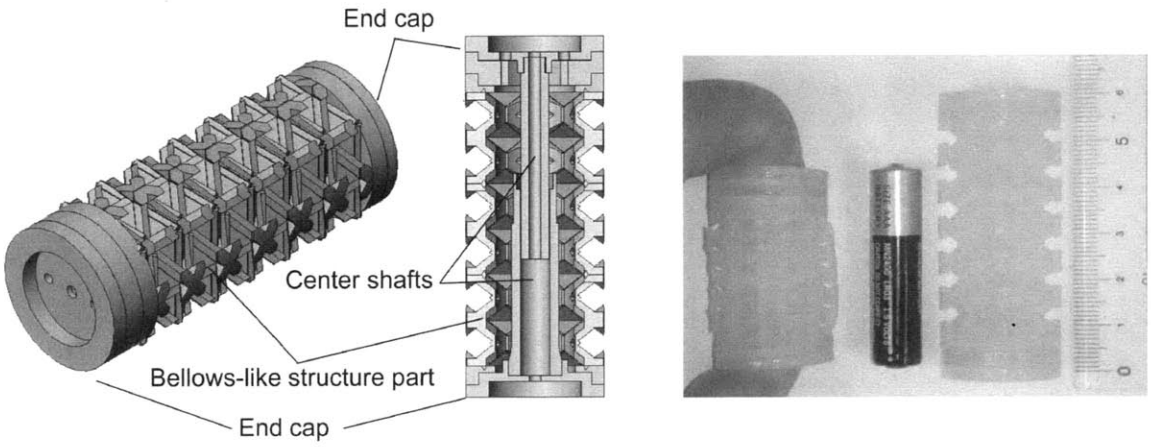

Figure 3: The prismatic joint in the current version of Squishbot[5].

It should be noted that while an ideal prismatic joint exhibits purely one-dimensional compliance, all structures have at least some compliance in their non-ideal directions. The design developed in this thesis aims to achieve a high enough ratio of bending stiffness to axial stiffness to achieve the needs of Squishbot. This includes supporting its own weight when cantilevered and resisting buckling when undergoing large compressive deformation.

The requirements of a mechanism that requires low actuation force at small scale and is assembly-free suggest the pursuit of a design that employs flexures. Significant work has been done in the theory of flexure design[6], but while flexures are well studied, there are several aspects of soft prismatic joint design that stray from traditional flexure design. First, flexures are not generally made of materials as soft as those used in this application. Where normally it can be assumed that the stiff direction of a leaf element is infinitely stiff, when working with soft materials at small scale, the stiff directions clearly have only finite stiffness. In addition, flexures are not often used in large-deformation applications. This means that the tools often used for

flexure design including finite element analysis become less helpful. Also, limited space and large deformations produce a challenge of how to achieve axial compression without accruing radial expansion. In addressing these problems, this thesis hopes to add to the knowledge of design of non-ideal, large-deformation flexures while also expanding the design platform for prismatic joints.

1.3 Design Requirements

The design requirements for this project are tailored to fit the needs of Squishbot. In order to fulfill the Chembot requirements, the joint must fit in a cylindrical envelope that is 4cm long and 1cm in diameter. The structure must compress 1.2cm axially without buckling and must support its own weight when cantilevered. Full compression should be achievable with linear actuation of less than 5N. The joint should also be low-weight and incorporate a restoring force of more than 1.5N. The joint must also be soft as defined above. The design requirements are shown in Table 1.

Table 1: Design requirements for the soft prismatic joint developed for Squishbot.

Design Requirements	
length	≤ 4cm
diameter	≤ 1cm
compression	≥ 1.2cm
deflection under own weight	≤ 1mm
material modulus	≤ 1GPa
weight	≤ 2g
force to actuate	≤ 5N
restoring force	≥1.5N
does not buckle	required
no assembly	required
low friction mechanism	required

1.4 Thesis overview

In describing the development of a soft prismatic joint, this thesis presents a design

process as well as the analysis and testing of a design. Chapter 2 describes the preliminary design stages in which the design strategy was chosen. This iterative process started with a decision to use flexures and evolved to the decision to use a screw design. Chapter 3 describes the further development of the screw design in which intuition and a series of qualitative testing were used to develop the design to the point where it was almost able to fulfill the design requirements of Squishbot.

Chapter 4 describes the development of a model describing the relationship between parameters and performance of the joint. This model was used to modify the joint design to fulfill the design requirements of Squishbot. The model developed in Chapter 4 was then tested in Chapter 5 against experimental date from 3D printed samples. The model was found to be adequate, predicting the axial to radial stiffness ratio of the joint to within a factor of three. Chapter 5 also presents modeling and testing of a final design of the soft joint with the desired dimensions and mass. The final design is capable of the required displacements, can support its own weight when cantilevered and does not buckle when compressed. It requires no assembly and does not produce internal friction when it deforms. The only requirement still left to be addressed is the restoring force value, which was too low in the tested models. This can be easily remedied by replacing the joint's material with a stiffer material. According to the model presented later, this change will not detract from achieving the other design requirements.

Chapter 6 describes conclusions and future work. Future work includes further refining the model and testing the model over a larger range of parameters. It also includes changing to a stiffer material and integrating the joint into the existing Squishbot robot. The development of a locking mechanism that can be used to disable the joint's axial degree of freedom is also suggested.

Chapter 2: Preliminary Design

2.1 Manufacturing Method

It was decided initially that all models would be prototyped using an Objet 3D printer, using TangoPlus as the material [7]. 3D printing was chosen as a manufacturing method because it is a rapid prototyping technique that is suitable for work with soft polymers. The Objet printer employed was a Connex500. It has a build space of 490 x 390 x 200mm and a resolution of 42 microns in the x and y-axis and 16 microns in the z-axis. TangoPlus was chosen as the material because of its low modulus of elasticity and its large elongation at break. It has a Young's modulus that ranges from 0.1MPa at 20% strain to 0.3MPa at 50% strain. TangoPlus has an elongation at break of 218%, allowing elements to fold a full 180 degrees without breaking. However, over time, TangoPlus becomes brittle and exhibits significant creep. For the purposes of prototyping, 3D printing with TangoPlus is ideal but the manufactured version should be injection molded out of a material such as polyurethane. Table 2 shows the properties of TangoPlus. Table 3 shows the material properties of C.U. E.'s PO645 polyurethane, one possible material for manufacture.

Table 2: Material properties of TangoPlus[8].

Property	ASTM	Metric	
Tensile Strength at Break	D-412	MPa	1.5
Modulus of Elasticity at 20% Strain	D-412	MPa	0.1
Modulus of Elasticity at 30% Strain	D-412	MPa	0.2
Modulus of Elasticity at 50% Strain	D-412	MPa	0.3
Elongation at Break	D-412	%	218
Compressive Set	D-395	%	4
Shore A Hardness	D-2240	Scale A	27
Tensile Tear Resistance	D-624	Kg/cm	3

Table 3: Material properties of PO645 Polyurethane[9].

Property	ASTM	Metric	
Tensile Strength at Break	D-412	MPa	15.9
Modulus of Elasticity at 50% Strain	D-412	MPa	0.6
Modulus of Elasticity at 100% Strain	D-412	MPa	0.8
Modulus of Elasticity at 200% Strain	D-412	MPa	1.2
Elongation at Break	D-412	%	700
Compressive Set	D-395	%	15
Shore A Hardness	D-2240	Scale A	47
Tensile Tear Resistance	D-624	Kg/cm	17.9

2.2 Concept Generation

As described in the introduction, it was decided that the design requirements of a soft prismatic joint lend themselves to a design employing flexures. From this point however, the design strategy must be further defined.

There are three main strategies for achieving the large (30%) axial deformations required by the design parameters. One strategy employs pure axial deformation as illustrated by a piece of rubber band. A design based on pure axial deformation depends on the use of a super-elastic material with a low Young's modulus and/or a small cross-sectional area. While this strategy is able to achieve large deformations given the proper material and geometry, the parameters needed to achieve large deformations result in a design with very low bending stiffness. Since a prismatic joint needs high stiffness in bending, this strategy was not pursued.

The second strategy uses combinations of 4-bar linkages oriented in such a manner that they cause the structure as a whole to stretch or compress when the links move relative to each other. This strategy can be illustrated by an accordion. Similarly, a third strategy illustrated by a spring, uses beam bending of a curved beam to produce compression of the structure as a whole. Since the second and third strategies both depend on beam bending to achieve structure compression, they can achieve higher deformations at lower forces than the first strategy while

also maintaining a high enough cross section and material modulus to be stiff enough in bending. For these reasons, the second and third strategies were pursued.

Four design concepts for the prismatic joint were created from these two strategies as shown in Figure 4. The linkage, bellows and screw are based on the second strategy and the spring design is based on the third strategy.

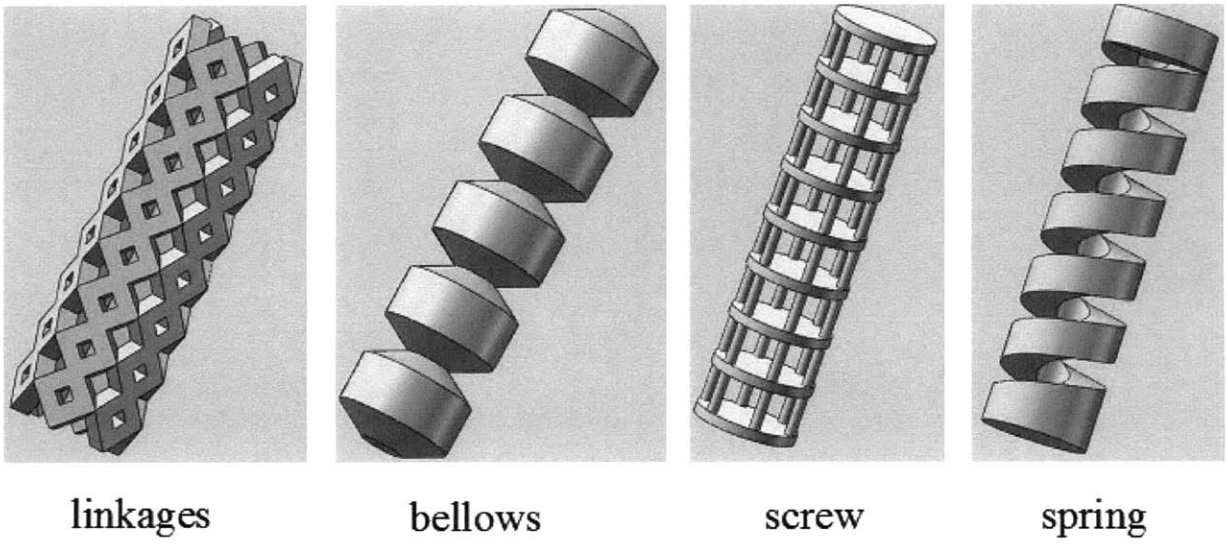

Figure 4: Four design concepts for a soft prismatic joint.

The three concepts based on 4-bar linkages can be differentiated by the orientation of the 4-bar linkages. Figure 5 illustrates the locations of the 4-bar linkages in the design and how the structure as a whole moves as the 4-bar linkages and deformed. In the linkage design, the 4-bar linkages are arranged in rings along the circumference of the structure. In the bellows design, the 4-bar linkages are swept about the center axis to form the sections of the bellows. In the screw design, the 4-bar linkages are arranged along the circumference of the structure. Unlike the linkage and bellows designs whose linkages compress simply when the structure is compressed, the screw's linkages skew when compressed. This means that axial displacement of the screw structure is coupled to rotational displacement.

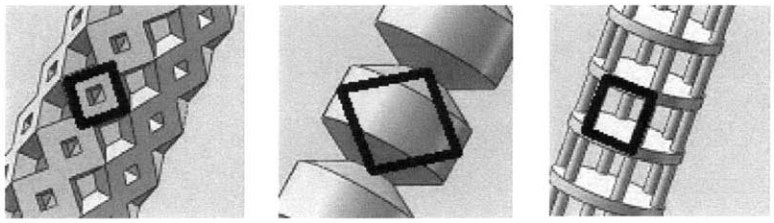

Figure 5: Location of the 4-bar linkages within three of the design concepts.

An embodiment of each design was 3D printed out of TangoPlus and tested qualitatively. When tested, the spring demonstrated high axial compliance, but also high bending compliance. In addition it demonstrated almost no restoring force. This behavior was predictable if one considers that even springs made out of stiff materials (like steel) exhibit considerable axial and bending compliance. It was determined that a spring made out of a soft material would not be able to achieve the desired stiffness in bending so this concept was abandoned.

The linkage design was able to achieve the desired compression and appeared to be stiff enough in bending. However, because the 4-bar linkages need to widen for the structure to compress, the structure expands radially in compression. In addition, in the embodiment investigated here, a significant amount of material must bend in order for the structure to compress. This requires large forces to achieve the desired displacement. While these problems could be fixed, they posed a large enough challenge that the concept was discarded.

The bellows design also achieved the desired compression. However, as with the linkage design, when the structure compressed, the structure expands radially. In addition, because a large amount of material needs to be deformed in order for the structure to compress, high forces are needed to achieve the desired compression. Moreover, the narrow regions between the sections of the bellows are very compliant in bending, allowing the structure as a whole to bend under low forces. For these reasons, the bellows concept was deemed unsuitable.

The screw design that was built and tested employed vertical rods and was actuated with a rotary force. The first version also used a stiffer 3D printed material, VeroWhite (modulus of

elasticity: 2495 MPa) for the rods. The straight orientation of the rods as well as their stiff material caused the structure to act very nearly to an ideal screw. This gave the screw a very high bending stiffness. In addition, since this structure twists to compress, it does not leave its 3D envelope in compression. Also, since very little material needs to deform in order for the screw to compress, it takes very low force to compress compared to the other designs. The structure also has enough restoring force to decompress with no actuation. While all of the designs possessed the potential to fulfill the design requirements, the screw design seemed to be the most promising, and so it was pursued. Figure 6 shows the results of the first round of qualitative testing.

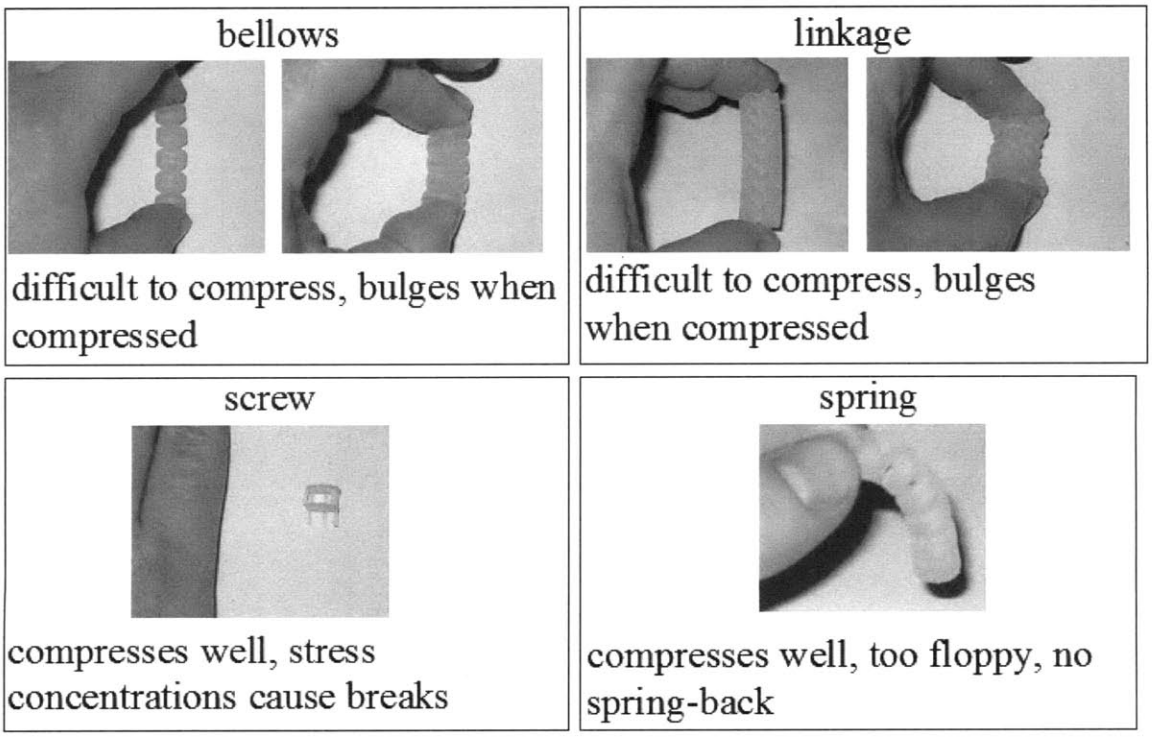

Figure 6: Results from qualitative testing of the four design concepts for the prismatic joint.

Table 4 shows a Pugh chart of the results. The Pugh chart employs a simple sponge as the datum. A sponge is used as the datum because it is a structure that is capable of large deformations, exhibits a restoring force and can be manufactured using a 3D printer. For

qualitative testing, a piece of a kitchen sponge was used in order to compare sponge behavior to the printed models.

Table 4: Pugh chart for the four concepts. A sponge is used as a datum.

	sponge	spring	linkage	bellows	screw
axial compliance	0	+	-	-	+
bending stiffness	0	-	+	+	+
axial expansion	0	+	-	-	+
restoring force	0	-	+	+	+

Chapter 3: Design Parameters of Selected Concept

The next step in the design process was to improve the screw design. One area of focus was finding a way to reduce the stress concentrations between the stiff rods and the compliant discs. While the stiff rods provide a large advantage in bending and do not compromise the movement of the joint in compression, preliminary testing showed that stress concentrations at the interfaces of materials with largely differing moduli of elasticity are largely intractable. The dual-material design was thus abandoned in favor of a single material design made entirely out of TangoPlus.

Other improvements to the screw design were implemented as shown in Figure 7 and Figure 8.

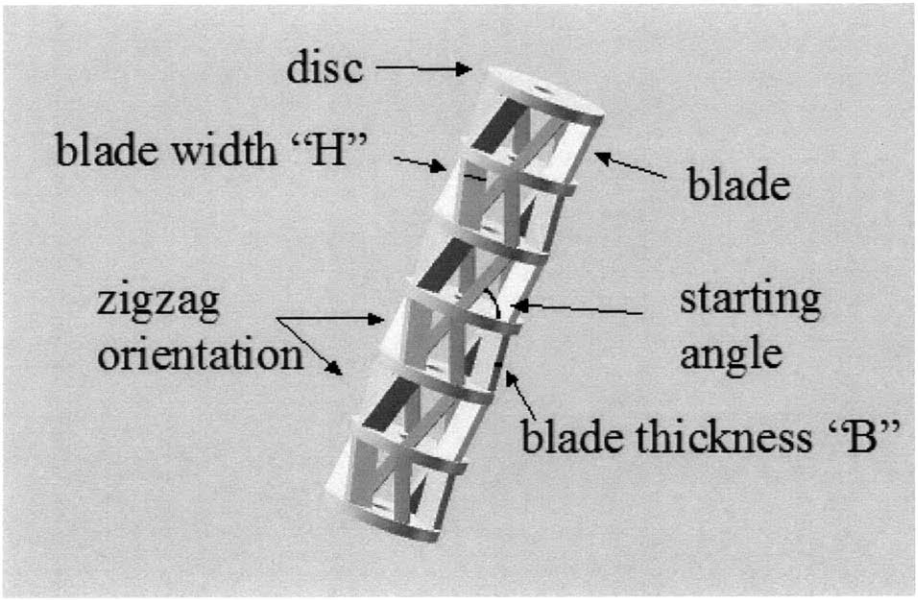

Figure 7: Screw improvements include exchanging blades for rods and implementing a starting angle.

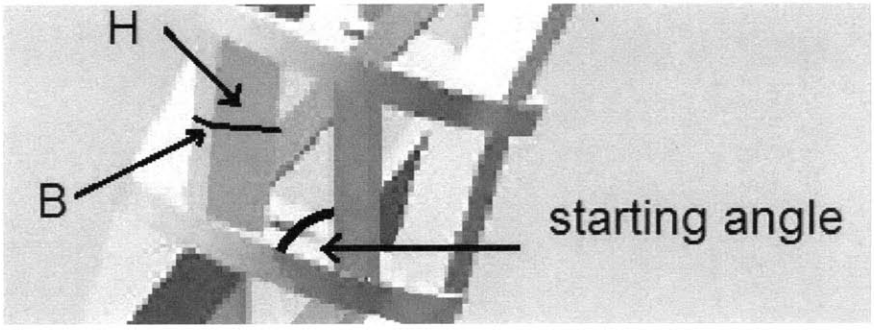

Figure 8: Close up of improved screw design.

Changing the rod material from the stiffer VeroWhite to the more compliant TangoPlus causes the structure as a whole to become less stiff in bending. In order to gain back this stiffness, the rods were extended into blades. In theory, this new geometry increases the rods' contribution to the stiffness of structure in bending. When the structure compresses, each blade folds over its compliant axis, providing little resistance to the motion. However, when the joint is loaded radially, the blades at the top and bottom of the joint are loaded radially about their stiff axis, causing the structure as a whole to exhibit increased stiffness in bending.

A starting angle for the blades was incorporated so that the screw could be actuated linearly. In the original screw design, the blades were oriented vertically so that the screw had to be actuated rotationally. While incorporating a starting angle reduces the overall allowable compression of the joint, the added functionality of linear actuation was deemed worthwhile.

With the implementation of a starting angle, the designer can now decide the direction that each layer of the screw rotates. Where before with the rotational actuation, all of the layers of the screw had to rotate in the same direction, with the starting angle the direction of rotation could be alternating layer by layer allowing the structure as a whole to have no net rotation when compressed. This also allows every second disc to have no rotation, hence there is a place to connect the feet that won't rotate.

With these changes, the design concept was finalized. A model of the final concept is shown in the in Figure 9. This prepared the stage for the next step in the design process of

quantitatively optimizing the concept.

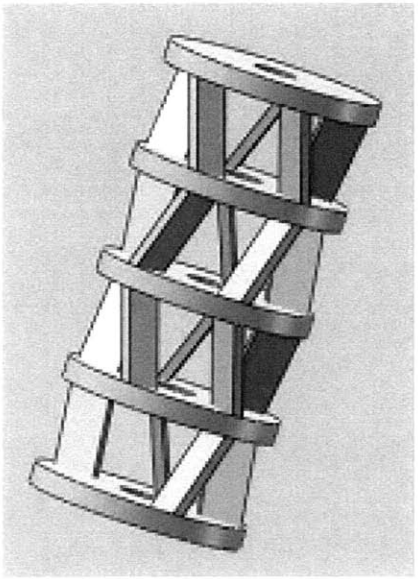

Figure 9: Final concept.

Chapter 4: Modeling

There are some definitions that will be used for rest of this thesis. A single layer of the joint consisting of a layer of blades and a single disc is considered a single "cell". This is a useful concept because if behaviors can be established for a single cell, they can be extended to describe a larger structure by considering combinations of cells in series and in parallel. A photograph of a single cell is shown in Figure 10.

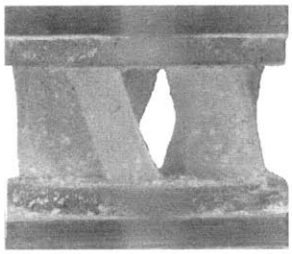

Figure 10: A single cell with stiff caps on the top and the bottom to help secure the sample.

When discussing designs, I_{eq} is defined as the area moment of inertia of the joint in bending. A_{eq} is defined as the cross-sectional area that a solid cylinder would need to possess to have the same stiffness in compression as the sample. The ratio of these two values, here called the "stiffness ratio", is used as a metric for the performances of the design. This metric can be used to determine how close a structure is to an ideal prismatic joint.

In addition, for this thesis, the labels I_x and I_y are used to discuss the area moments of inertia of a single blade. I_x is the area moment of inertia of a blade in its stiff direction and I_y is its area moment of inertia in the compliant direction. These conventions are shown in Figure 11.

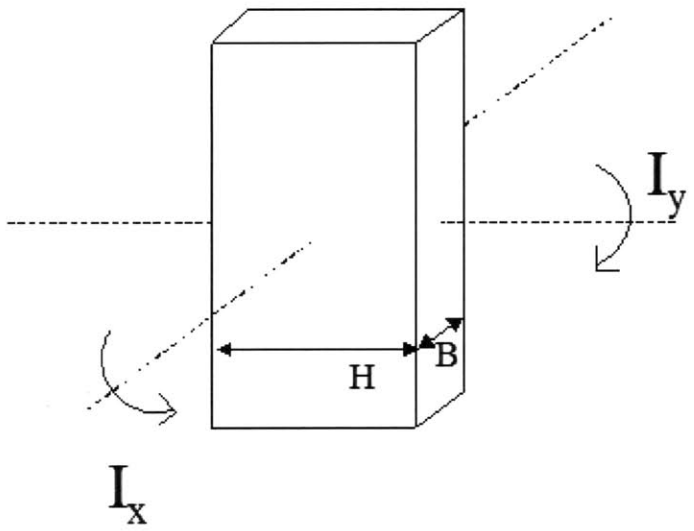

Figure 11: Area moment of inertia conventions for a blade.

After choosing the screw concept, the design was evaluated and optimized. A model of the design was presented and evaluated. The model presents a mathematical relationship between the parameters (blade dimensions, starting angle etc) and the performance of the joint. A verified model of this type would allow the parameters to be adjusted in order to tune the performance of the joint as a whole. It is also desired to be able to predict if a design will fulfill the defined design parameters based on the performance of a single cell or pair of cells. This chapter presents a metric for this use.

The proposed model is as follows: In compression, a single cell behaves as a group of beams all bending over their own compliant axes. In bending, the structure acts as a single beam bending along its stiff direction over a neutral axis a half radius from the center of the ring. The bending model is illustrated in Figure 12.

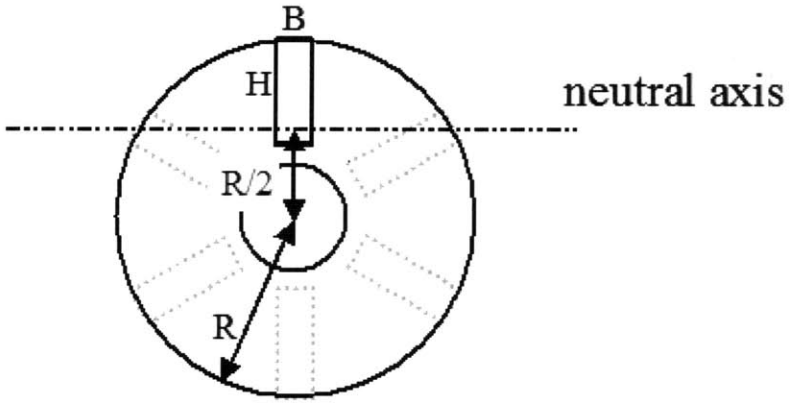

Figure 12: Ring model for structure in bending

This model was arrived at based on qualitative observations of the test cells. The model for axial compression was decided on based on observation and intuition. The model for bending is less intuitive and was arrived at as follows: As is always the case in bending, if a radial load is applied to a cell, one side is put into tension and the other side is put into compression. In this case, the cells were observed to bend over a neutral axis midway between the center axis of the cell and the tensioned edge of the cell. It was also observed that the blades on the compressed side of the cell did not hold their original orientation under load but rather folded along their compliant axis. This suggests that the only resistance to bending comes from the blade or blades on the tensioned side of the cell.

This model can be codified into equations as follows: Using the equation for bending of a cantilevered beam, deflection of a blade when the joint is loaded axially can be expressed as

$$\delta_{blade} = \frac{F_{total} L_{blade}^{\ 3} \cos(\theta)}{3SEI_y} \tag{1}$$

where δ_{blade} is the deflection of the blade, F_{total} is the axial force applied to the joint as a whole, L_{blade} is the length of a single blade, S is the number of blades per cell, θ is the angle of the blade from the horizontal and E is the Young's Modulus of the material. I_y is the moment of inertia of a blade in its compliant direction and is defined as

$$I_y = \frac{HB^3}{12}. \tag{2}$$

S appears in Equation (1) because F_{total} is spread over S blades in parallel. The $\cos(\theta)$ in Equation (1) accounts for the fact that the load is not radial to the blade.

Using the equation for axial displacement, deflection of the joint as a whole in compression can be expressed as

$$\delta_{total} = \frac{F_{total} L_{total}}{EA_{eq}} \tag{3}$$

where δ_{total} is the deflection of the joint as a whole, L_{total} is the length of the whole joint, and A_{eq} is the equivalent cross-sectional area of the joint as defined earlier. δ_{blade} and δ_{total} can be related according to

$$\delta_{total} = \delta_{blade} \cos(\theta). \tag{4}$$

Putting these Equations (1), (3) and (4) together an equation for A_{eq} is established, given by

$$A_{eq} = \frac{3SI_y L_{total}}{\cos^2(\theta) L_{blade}{}^3}. \tag{5}$$

Using the model for bending where the entire load in bending is supported by a single blade, I_{eq} can be expressed as

$$I_{eq} = I_x + HB\left(\frac{R}{2} - \frac{H}{2}\right)^2 \tag{6}$$

where R is the radius of the structure and I_x is defined as

$$I_x = \frac{BH^3}{12}. \tag{7}$$

The second term of Equation (6) is derived using the parallel axis theorem, assuming that the neutral axis is half a radius from the outer edge of the joint.

Combining Equation (5) and (6), the stiffness ratio of the structure as a whole can be

modeled as

$$\frac{I_{eq}}{A_{eq}} = \frac{\left(I_x + HB\left(\frac{R}{2} - \frac{H}{2}\right)^2\right) L_{blade}{}^3 \cos^2(\theta)}{3SI_y L_{total}}. \tag{8}$$

The model was evaluated assuming a constant blade angle of 45 degrees. This assumption is based on the idea that if used in the robot, the joint would be preloaded such that all displacements were centered about a blade angle of 45 degrees. The assumption of a constant angle introduces a maximum multiplicative inaccuracy of four into the calculated stiffness ratio as shown in Figure 13. However, since these are only first order models used to gain insight into the behavior of the design, this level of inaccuracy is acceptable.

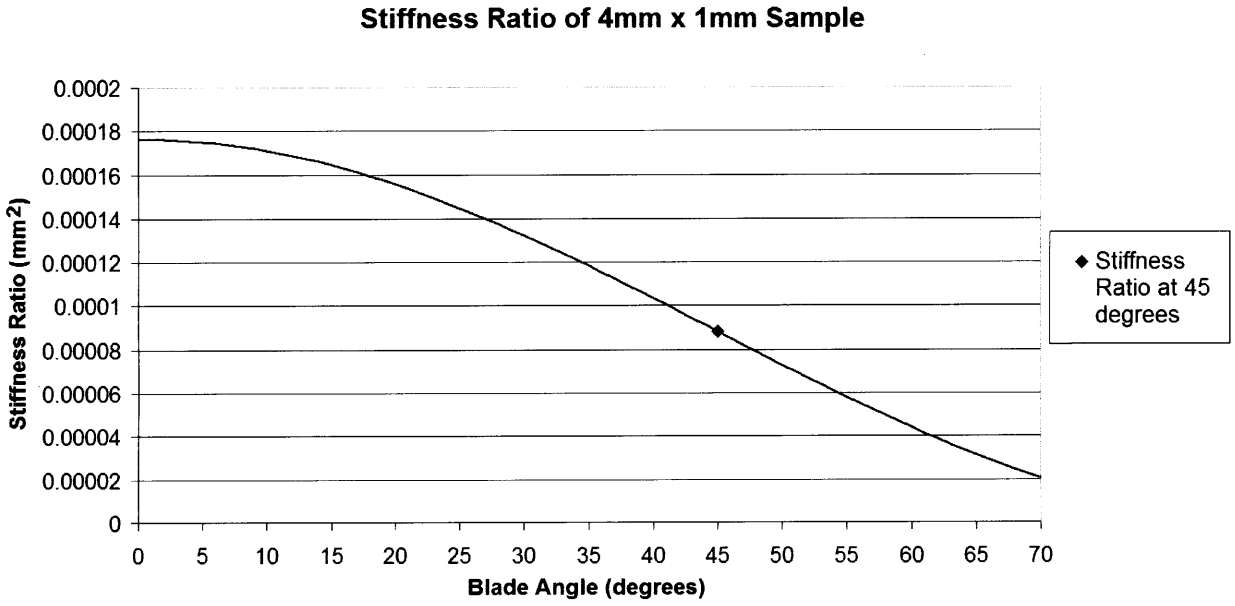

Figure 13: Stiffness ratio as a function of blade angle

With the model established, the stiffness ratios predicted by the model can be compared to the measured stiffness ratios of the samples. These results will be presented in the results chapter.

It is also desired to be able to predict if a design will fulfill the defined design parameters based on the performance of a single cell or pair of cells. This can be achieved by substituting

the measured behavior of a sample into the buckling equation. Assuming concentric loading, the buckling equation states that in order not to buckle

$$F_{total} < \frac{\pi^2 EI_{eq}}{L_{total}^{\ 2}} \tag{9}$$

must be true.

Substituting

$$L_{total} = \frac{\delta_{total}}{\varepsilon_{total}} \tag{10}$$

into Equation (9) where ε_{total} is the strain of the joint in compression expressed as a decimal and δ_{total} is the desired compression defined by the design requirements, the equation as a whole can be rearranged to be written as

$$\frac{F_{total}}{EI_{eq}\varepsilon_{total}^{\ 2}} < \left(\frac{\pi}{\delta_{total}}\right)^2. \tag{11}$$

In this form, the left hand side of the equations is determined by measurement and the right hand side of the equation is determined by the design requirements. Results from evaluating Equation (11) are presented in the results chapter.

Chapter 5: Experimental Setup and Results

5.1 Test Sample Design

While the screw design has many parameters that can be varied, the experimenter focused on the effects of changes in blade dimension thickness, "B", on joint performance. In order to test the effects of blade width on performance, there are many parameters that must be held constant. These values were largely determined through intuition and preliminary experiments. The number of blades per cell was decided based on the observation that only a small range of number of blades per cell is practical to manufacture. This range spans from three blades per cell, below which there is no hope for bending stiffness, to six blades per cell, above which there is not enough room in the cell for the blades to compress fully. It was decided to use five blades per cell, as this value produced behavior in an appropriate range of maximum compression and axial stiffness.

The effect of relative angular orientations of the cells layer by layer was also observed qualitatively. Samples exhibiting two possible orientations of the layers are shown in Figure 14. No significant difference in behavior was observed between the two samples so the choice to use the straight configuration was made without further data.

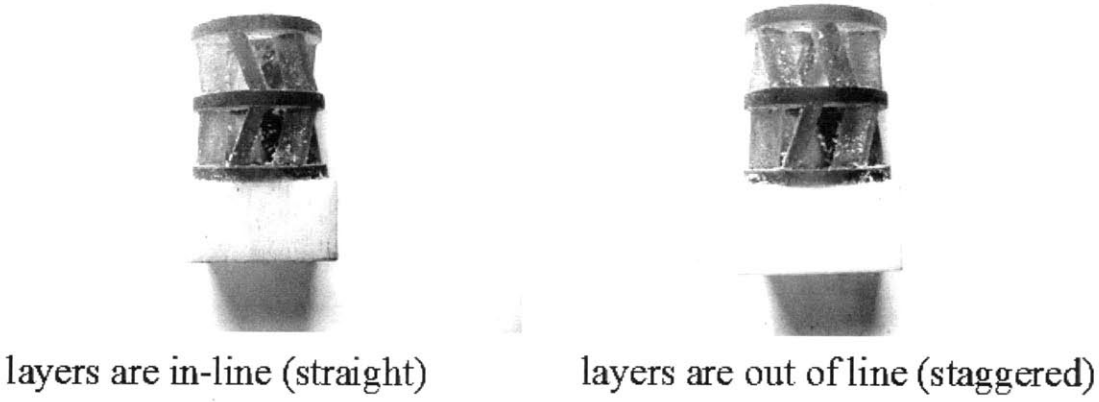

Figure 14: Straight versus staggered layer-by-layer cell orientations.

Several other parameters were defined through intuition. The height of the cells was set at 5mm. This parameter was decided in conjunction with the decision about the number of blades per cell. Taller cells allow higher overall compression of the joint. However, if the cells are too tall, the blades will be long enough that they will interfere with each other when the cell is compressed. The height at which this becomes a problem is thus related to both the cell height and the number of blades per cell. The combination of 5mm cell height and 5 blades per cell provided enough room for the cell to compress fully so those values were used.

Disc-thickness was set at 1mm. A trade-off exists for this parameter. Because the discs act as a dead space for compression, the thicker the discs, the lower the allowable compression of the cell. However, if the discs are too thin, it was observed that their high compliances compromise the bending stiffness of the joint overall. This is because the compliant disc folds and twists into a position where the blades are no longer oriented in their stiff direction. Similar reasoning was used to set the diameter of the hole in the center of the discs to 2mm. This hole is needed for the actuator. However, if the hole is too large, the disc loses its stiffness resulting in the increased bending compliance described above.

The starting angle of the blades was set to 70 degrees. This value was set using intuition. Again there is a trade-off. A high starting angle allows room for a larger maximum axial compression of the cell. However, a high starting angle also means a higher axial stiffness of the cell because of the high angle between the blade and the force that must bend the blade.

Limits on blade width and thickness were also observed. It was found that with 5 blades per cell, any blade geometry with a width of more than 2mm produced interference between blades when the structure was compressed. This caused an instability of the structure. It was therefore decided to limit blade width to 2mm. It was also found that a blade thickness of 0.5mm was the minimum thickness that could be 3D printed with accuracy. This observation set the lower limit for blade thickness.

Seven test models were printed for the experiments. It was decided that tests would be conducted on samples made up of pairs of cells. A test sample is shown in Figure 15. Pairs of cells were used instead of single cells to ensure that the length to radius ratio of the samples was high enough for the tests measure bending and not shear. In addition, all test models were 3D printed at two times full-size in all dimensions in order to facilitate accurate measurement of deflections. Since the parameters cited in the previous paragraph apply to the full-scale model, the test samples have cell height of 10mm, disc thickness of 2mm and blade width of 4mm. Stiff, square plates were printed onto the bottom and the top of the test models to facilitate proper constraint in testing.

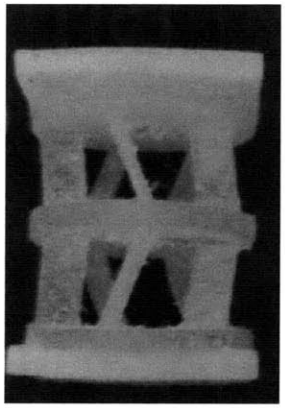

Figure 15: Test sample made up of two cells plus an additional disc at the bottom and hard plates on either end.

5.2 Instrumentation and setup

Instrumentation and setup of the compression and bending tests are shown in Figure 16 and Figure 17. Axial stiffness was tested by measuring displacement while applying a compressive axial load of known value to a pair of cells. Bending stiffness was tested by measuring radial deflection of the free end of a cantilevered pair of cells while applying a known radial load at the free end.

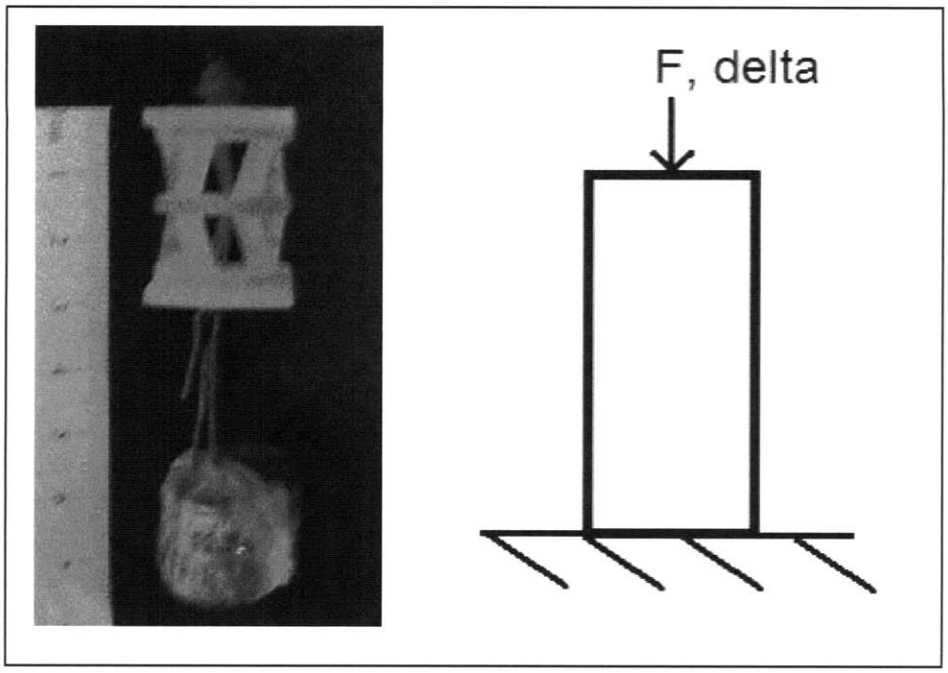

Figure 16: Photograph and schematic of the compression test setup.

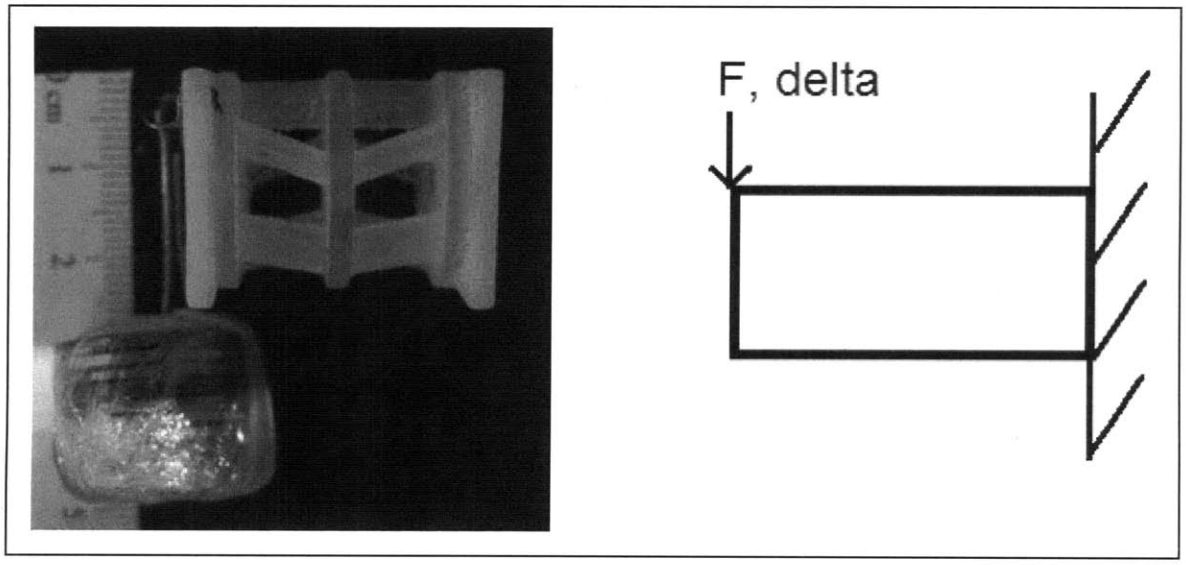

Figure 17: Photograph and schematic of the bending test setup.

Additional preliminary bending tests were conducted by loading the cell-pairs non-concentrically and measuring the angle made by the top of the upper disc as shown in Figure 18. While this non-concentric loading examines a realistic scenario, the combined bending and compression loads bending loads inherent to this test insert too much unnecessary complexity

into the results. This line of testing was thus abandoned in favor of the two more pure loading tests described above.

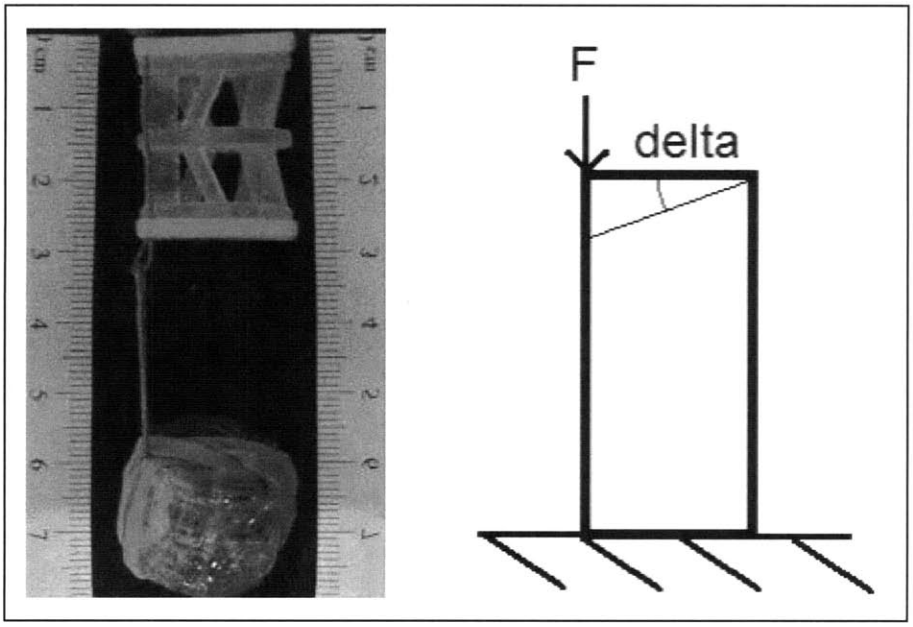

Figure 18: Photograph and schematic of the non-concentric loading test.

5.3 Results and Model validation

The model predicts that blade geometry plays an important role in the performance of the joint. In order to test this hypothesis, data was collected for seven cell-pairs each with different blade thicknesses. The set of blade thickness tested are shown in Figure 19.

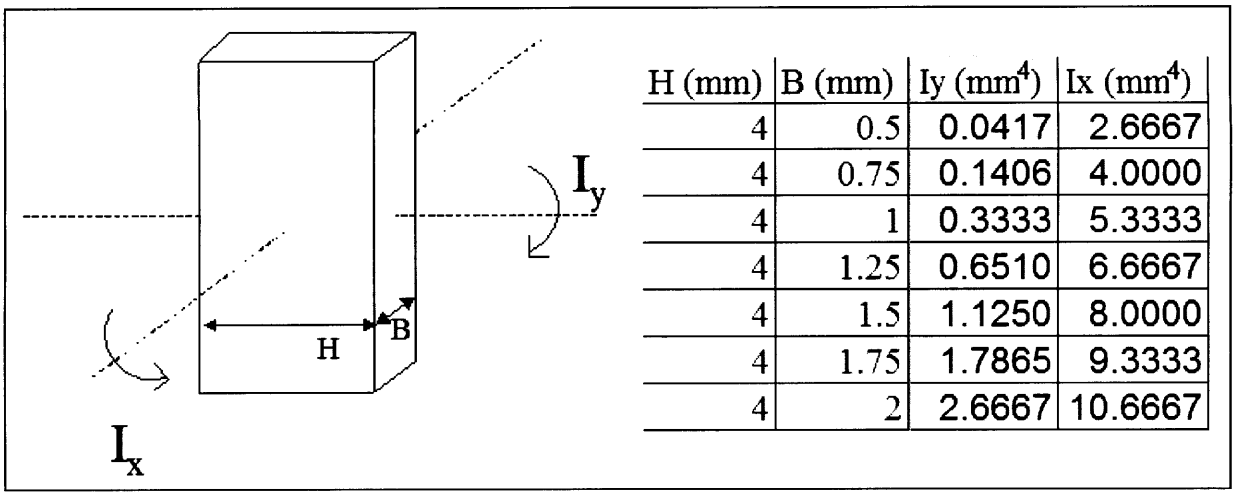

H (mm)	B (mm)	Iy (mm^4)	Ix (mm^4)
4	0.5	0.0417	2.6667
4	0.75	0.1406	4.0000
4	1	0.3333	5.3333
4	1.25	0.6510	6.6667
4	1.5	1.1250	8.0000
4	1.75	1.7865	9.3333
4	2	2.6667	10.6667

Figure 19: Blade dimensions and area moments of inertias of all samples.

Figure 20 shows the results of the compression tests. Compression tests were conducted in order to establish the relationship between axial compressive force and axial displacement. Each line represents a single sample with the legend indicating which sample goes with which dataset. Measurement errors in the x-axis were $\pm 0.5mm$ based on the limits of measurement capability using a ruler. The force values on the y-axis were measured using a scale and are accurate to within 0.02N.

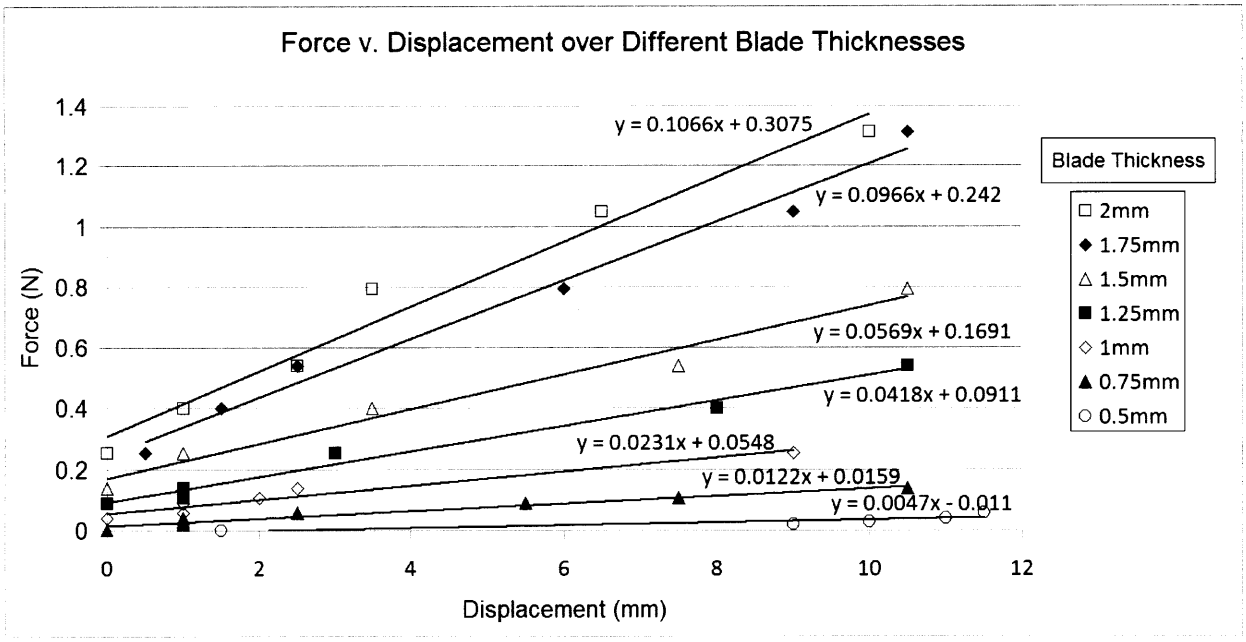

Figure 20: Force v. displacement in compression. Each dataset represents a blade thickness.

From the results of the compression tests, it is possible to calculate the axial stiffness of the structure and hence the measured EA_{eq}. Figure 20 only shows the linear range of sample compression: the range in which the sample compresses freely in a screw motion. Higher forces produced additional displacement caused by material deformation of the discs and the fully flattened blades. Hysteresis of up to 0.3N was observed in the stiffer samples. This could be the result of the high (70 degree) starting angle of the blades, which causes an initial inefficient transmission of force to displacement. It is also noted that the 4mm x 0.5mm sample has a negative y-intercept. This is because the sample is so compliant that it compressed under its own weight without any applied force.

Figure 21 shows the results of the bending tests. From the results of these tests, it is possible to calculate the bending stiffnesses of the samples and hence the measured EI_{eq} of each sample. As with the compression chart, each line represents a single sample, and the legend indicates the blade thickness of that sample. Measurement errors for displacement were again

determined to be $\pm 0.5mm$. The force values were again measured using a scale and are accurate to within 0.02N. Less than 0.05N hysteresis was observed in these tests and what was observed was attributed to measurement error.

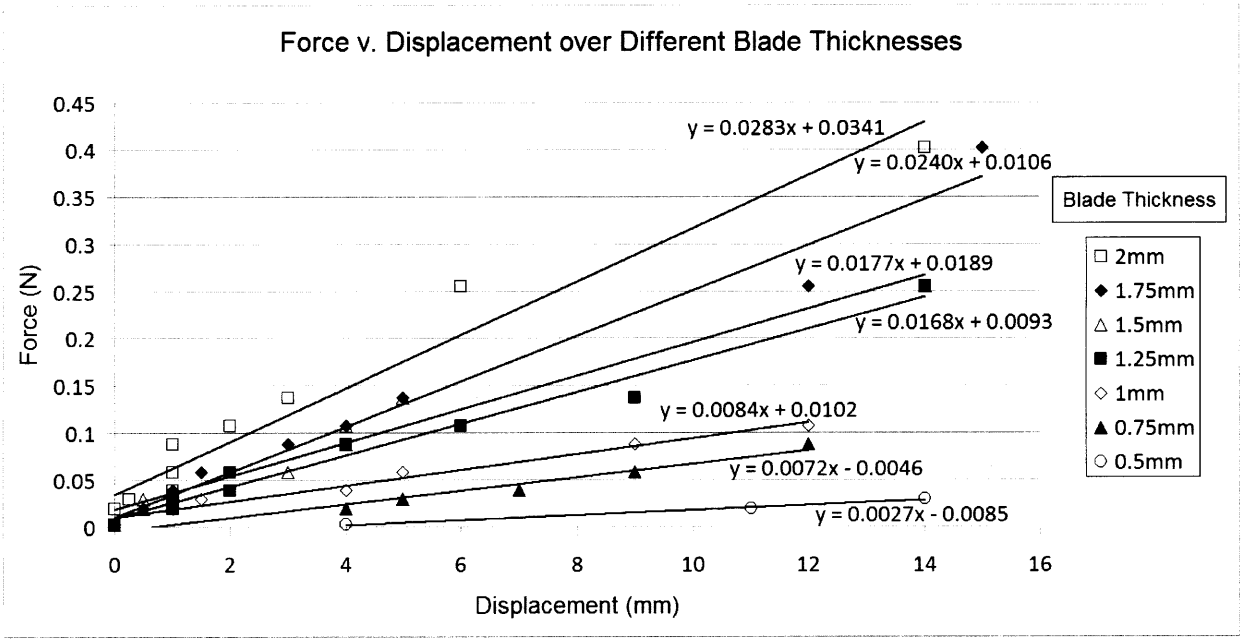

Figure 21: Force v. displacement in bending. Each dataset represents a blade thickness.

Figure 22 shows a plot of maximum strain versus blade dimensions. It was observed that maximum strain of the samples increased with decreased blade thickness. This was expected since compressed cell height is limited by the height of the discs plus the flattened height of the blades. Thin blades thus allow the cell to compress further than thick blades. The error bars for these results are larger than for the previous graphs because of the difficulty in determining the maximum displacement that is still within the linear range of compression. The error bars reported here were determined based on the resolution of the tests conducted.

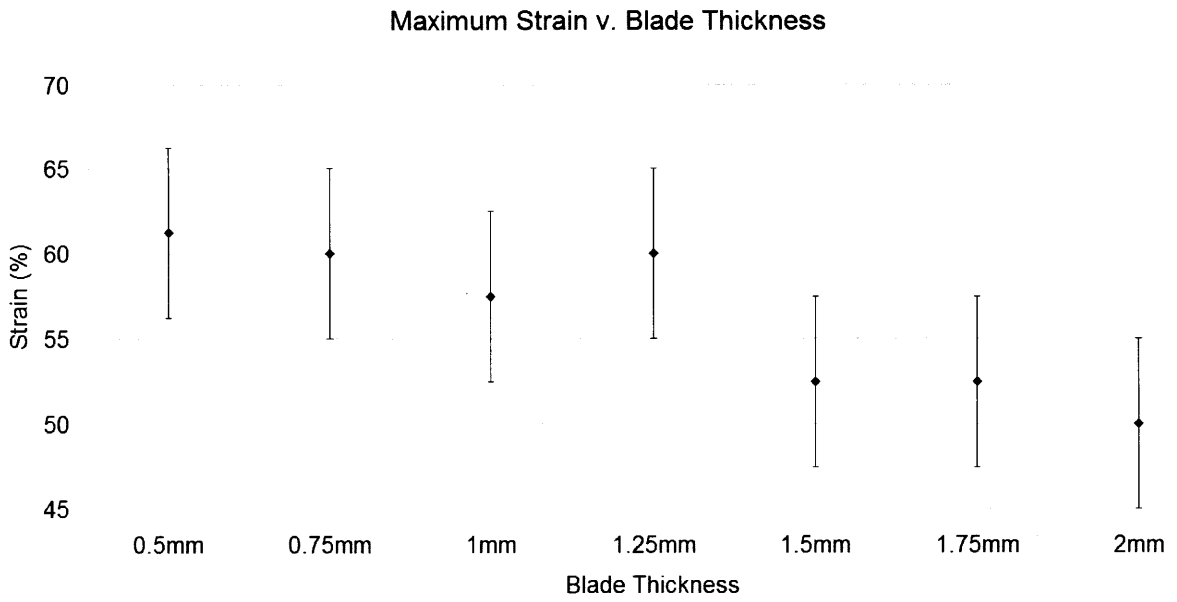

Figure 22: Maximum strain versus blade thickness.

Figure 23 shows the force needed by each sample to achieve maximum compression. It was found that the axial force necessary to fully compress the sample increases with blade thickness. This was predicted by the equations given above for $EA_{eq.}$ The error bars are large because of the difficulty in determining the maximum force in the linear range of compression. The error bars reported here were determined based on the resolution of the tests conducted.

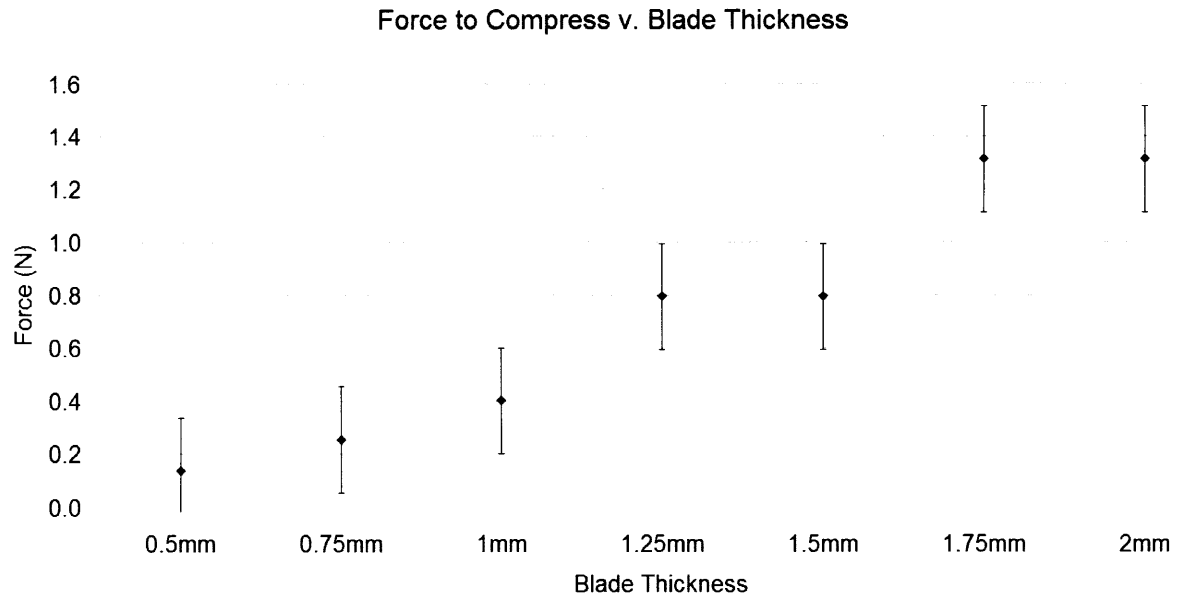

Figure 23: The force needed to fully compress the sample versus blade thickness.

Figure 24 compares the measured and calculated values of the stiffness ratio for each sample. The measured dataset was calculated using the results from the compression and bending tests reported above. The calculated dataset was computed according to the equations described in the previous chapter. Error bars are based on the errors accumulated between the compression and the bending tests as well as the uncertainty inherent in finding a linear fit for the axial and bending data.

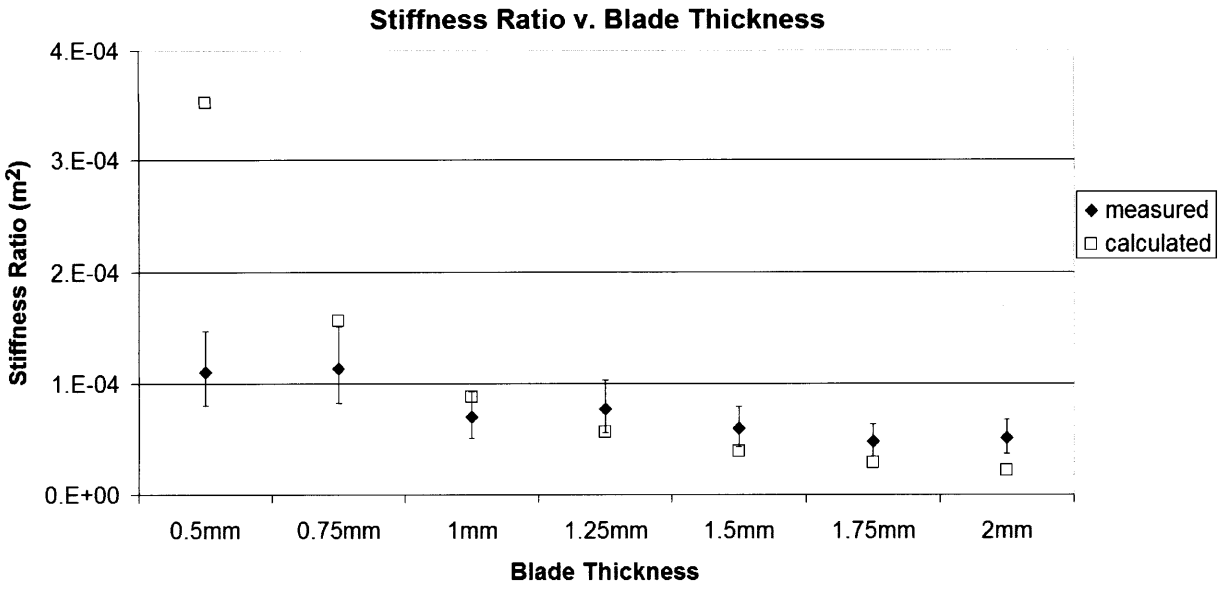

Figure 24: Calculated and measured stiffness ratio versus blade thickness.

Figure 24 shows that the calculated stiffness ratio is within a factor of three of the measured results. As the blades become narrower, the calculated values diverge from the measured data, suggesting that future work must be done to further develop the model. In addition, the calculated ratios for the larger blades are lower than what was measured again suggesting future work on the model.

Figure 25 shows the results from testing the buckling metric established in Equation (11). The data from the previous tests were gathered to determine if the samples would pass the buckling test if built to full height as defined by the design requirements. The y-values of the data points are calculated from the measured values reported above. Y-values for the samples are given by the left hand side of Equation (11)

$$\frac{F_{total}}{EI_{eq}\varepsilon_{total}^{2}}.$$

The grey region at the bottom of the chart is the region where a data point must be in order for

the sample not to buckle when built to full height. The upper bound of this region is defined by the right hand side of Equation (11)

$$\left(\frac{\pi}{\delta_{total}}\right)^2$$

where δ_{total} is set by the design requirements and equals 24mm. This value is twice that reported in the design parameters because the samples are two times larger than full-size. This is valid because buckling scales with size such that a geometry that does not buckle at double size will also be fine at normal size.

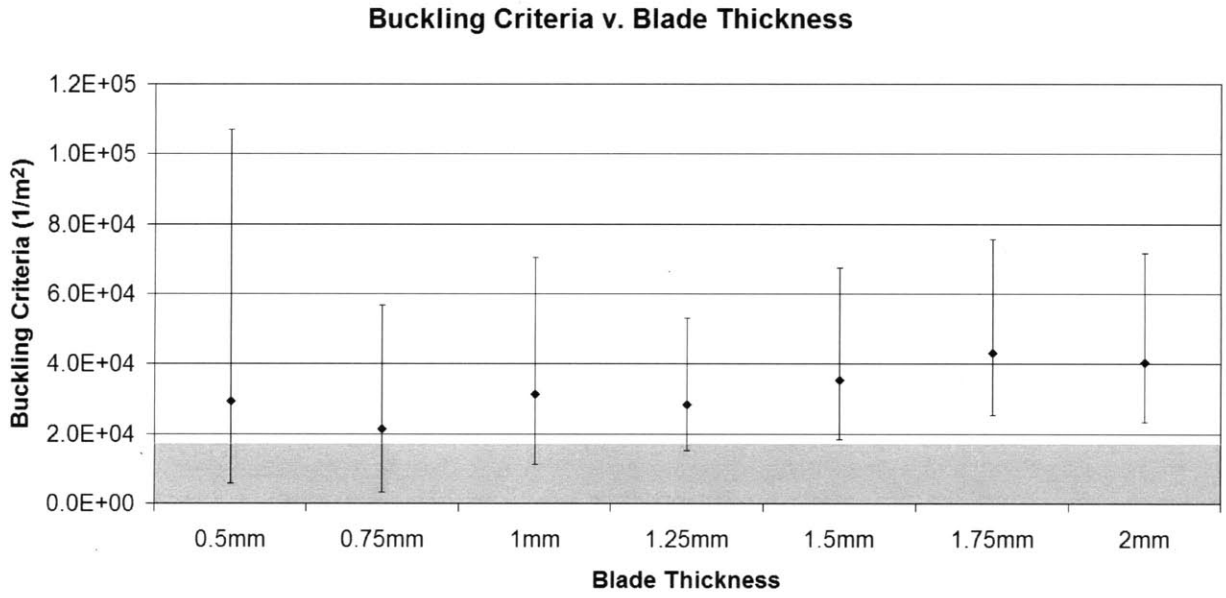

Figure 25: Buckling criteria versus blade thickness. If a sample falls within the grey region, it will not buckle.

As can be seen, none of the data points are within the non-buckling range. However, if we take into account the uncertainty of the data as shown with the error bars, it is possible that the first four samples would not buckle if built to full height. Based on these results, the 1mm sample was chosen as the best-behaved sample. This blade thickness was chosen because it was within the range of samples that could potentially resist buckling and, unlike the thinner samples which were fragile and difficult to constrain fully, it was well-behaved and easy to work with.

5.4 Full scale testing

A full-scale, full-length model was built using a 1mm thick blade. Note however, that when reduced to 1x scale from the 2x scale model, blade thickness was reduced 0.5mm. It was found through testing that the full-scale joint did not buckle and was able to achieve the specified design requirements with the exception of the restoring force. Table 5 shows the results of the full-scale experiments

Table 5: Results of full-scale experiments.

	desired	actual
length	≤ 4cm	2.3cm
diameter	≤ 1cm	1 cm
compression	≥ 1.2cm	1.2cm
deflection under own weight	≤ 1mm	≤ 0.5mm
material modulus	≤ 1GPa	0.2MPa
weight	≤ 2g	1g
force to actuate	≤ 5N	0.2N
restoring force	≥1.5N	0.2N
does not buckle	required	achieved
no assembly	required	achieved
low friction mechanism	required	achieved

Chapter 6: Conclusions and Future Work

The goals of this thesis were achieved: A soft prismatic joint was designed for Squishbot and a model that allows the design to be modified for other applications has been developed. Table 6 shows the parameters used in the full-scale version of the joint and Figure 26 shows a technical drawing of the full-scale joint. The soft prismatic joint developed and analyzed in this thesis employs a screw design, a strategy that was chosen after careful consideration of the available options.

Table 6: Final design parameters.

Number of cells	4
Num. of blades/cell	5
Total length	23mm
Cell height	5mm
Total diameter	10mm
Blade shape	2mm x 0.5mm
Starting angle	70 degree
Material	TangoPlus
Disc thickness	1mm

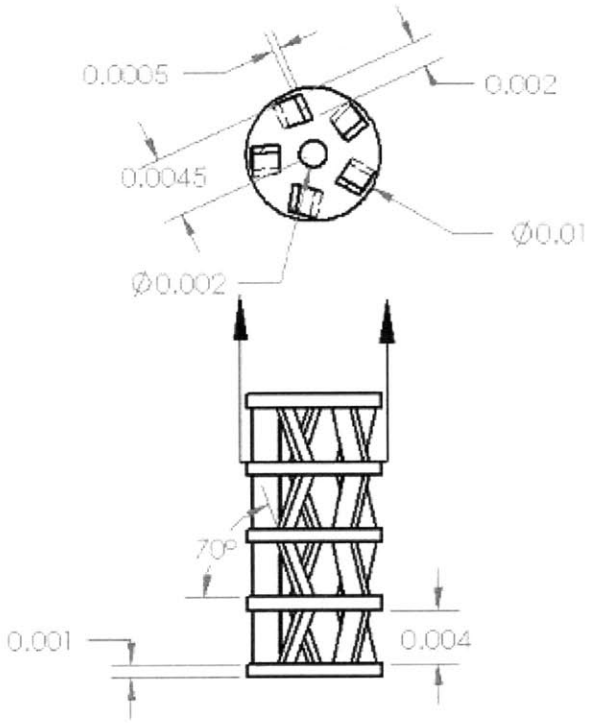

Figure 26: Final model of prismatic joint with all dimensions expressed in meters.

In this thesis, sample cells were tested against the model over the blade thickness parameter space in order to verify the model and determine the optimal parameters for Squishbot. The final full-scale model was also tested against the original design requirements. Figure 27 and Figure 28 show the results from testing of the full-scale joint.

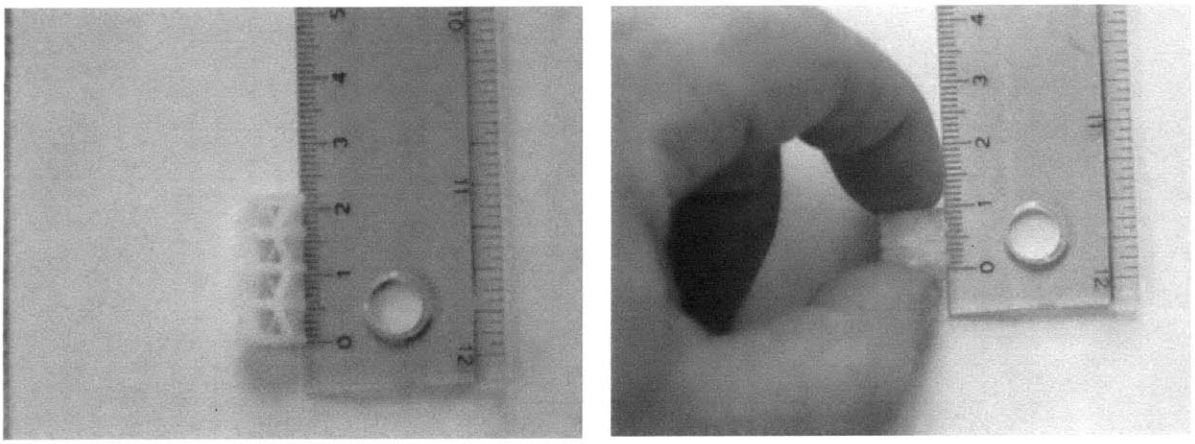

Figure 27: Results from testing the full-scale joint in compression.

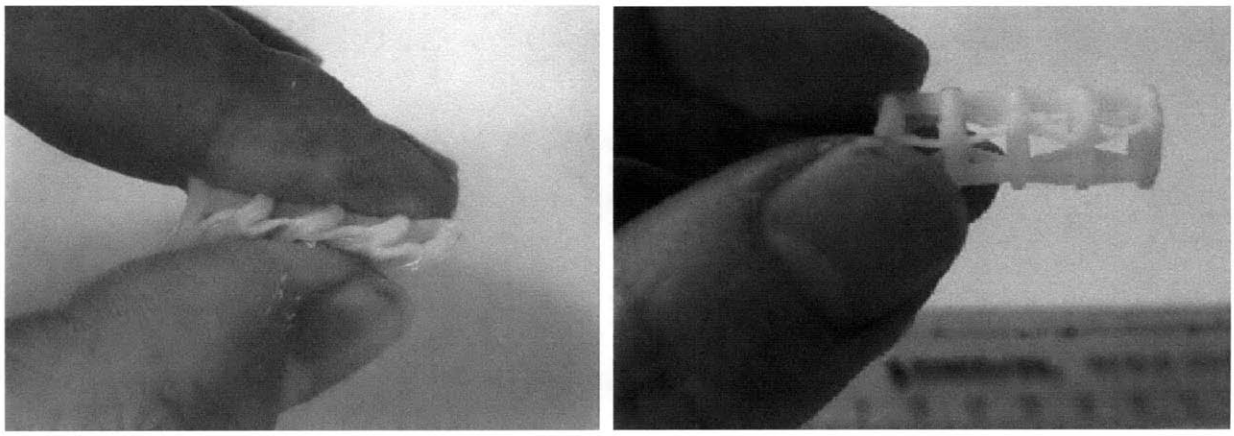

Figure 28: Results from testing the full-scale joint for softness and as a cantilever.

There are several steps that need to be taken to carry this project forward. The first goal is to increase the restoring force of the joint such that it is the in the correct range. This can be achieved by increasing the Young's modulus of the sample material. According to the model, increasing the modulus of the material does not affect the stiffness ratio of the joint. Increasing the material stiffness of the joint will increase the softness metric of the joint and the force needed to actuate it. Both of these values are well below their maximum thresholds so this solution is predicted to be a success.

Future work is also needed to integrate this joint design into a working robot. Consideration must be taken regarding how and where to attach feet, how to actuate the joint and how to connect the joint to the rest of the robot. In addition, this joint needs to be evaluated for durability over repeated use.

More work needs to be done to improve the accuracy of the model so that it describes the observed behavior of the joints more closely. A few ways to improve the model have been considered but not yet implemented. Firstly, the position of the neutral axis is currently established by qualitative observation. However, it appears that the neutral axis changes position proportionally to the ratio of I_x/I_y with it moving outwards from the center of the joint as I_x/I_y increases. If this observation were formalized in the model, it is likely that the calculated

stiffness ratios would better follow the observed stiffness ratios.

The model also assumes that only one blade carries the load in bending. This assumption appears to be true for five-blade cells but will not hold if the number of blades per cell is varied. The relationship between the number of blades holding the load and the number of blades per cell should also be investigated.

In addition, the effect of other parameters on the performance of the joint should be studied. Blade thickness has been investigated to the limits allowed by geometry and manufacturing capability. Other parameters to investigate include cell height, disc thickness, starting angle and building material. As these parameters are investigated, new properties and behaviors of the joint will emerge and the equations describing the joint's behavior can be modified.

In addition, the screw design invites the creation of a locking mechanism that is triggered by a rotational actuator and when activated, prohibits compression. Preliminary work was done on the development of the locking mechanism shown in Figure 29 and Figure 30. This mechanism employs legs made out of a stiffer 3D printed material, VeroWhite. With a slight twist, the legs can be brought into a position where they are pressed against each other, preventing the structure from compressing.

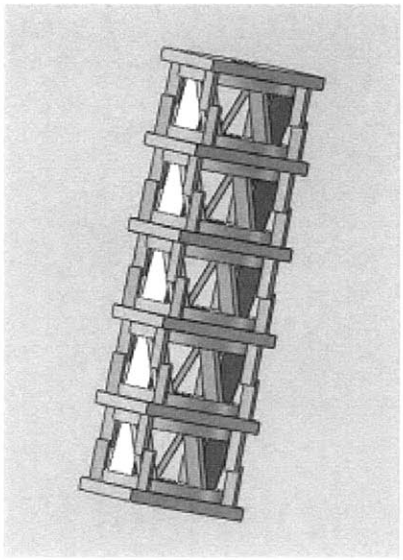

Figure 29: Model of locking mechanism in its unlocked state.

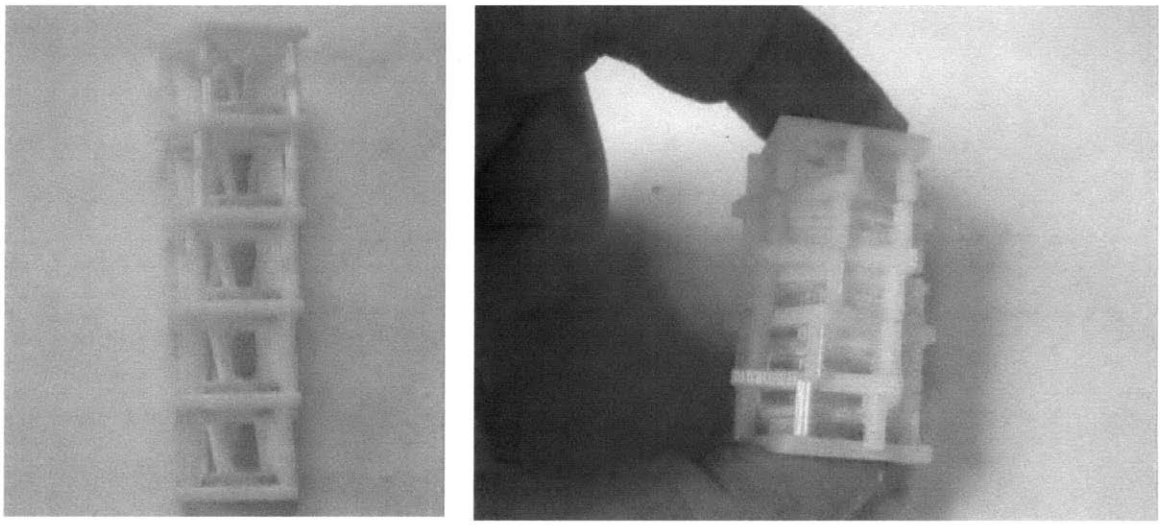

In locking mode

Compressed

Figure 30: Locking mechanism shown locked open (left) and fully compressed (right).

The largest challenge in designing a locking mechanism is to produce a mechanism that is made of the same soft materials as the rest of the structure. One such method is have a means to twist the structure into an orientation where the blades are parallel to the axis of the structure so that they are loaded axially when the joint as a whole is in compression. While this method works in theory, the blades used in the final implementation of the screw design would buckle under the actuator's load if oriented in such a manner. Since buckling is undesired, more work

needs to be conducted in this area.

With the successful fulfillment of the project's design goals, the work presented in this thesis is a valuable addition to the Squishbot project. In addition, the work presented here adds to the platform of soft prismatic design and can be used for future soft robotics development. This project invites a host of future work, indicating that is a rich area for future research. The design presented in this thesis is almost ready for integration into Squishbot, an existing soft robot. Future work could complete this integration and enable this design to be applied to other soft robots.

References

[1] http://www.darpa.mil/dso/thrusts/materials/multfunmat/chembots/index.htm

[2] Cheng, N., Ishigami, G., Hawthorne, S., Chen, H., Hansen, M., Telleria, M., Playter, R., and Iagnemma, K., "Design and Analysis of a Soft Mobile Robot Composed of Multiple Thermally Activated Joints Driven by a Single Actuator," IEEE International Conference of Robotics and Automation, 2010.

[3] Telleria, M., Hansen, M., Campbell, D., Servi, A., and Culpepper, M., "Modeling and Implementation of Solder-activated Joints for Single-actuator, Centimeter-scale Robotic Mechanisms," IEEE International Conference on Robotics and Automation, 2010

[4] Cheng, N., Ishigami, G., Hawthorne, S., Chen, H., Hansen, M., Telleria, M., Playter, R., and Iagnemma, K., "Design and Analysis of a Soft Mobile Robot Composed of Multiple Thermally Activated Joints Driven by a Single Actuator," IEEE International Conference of Robotics and Automation, 2010.

[5] Cheng, N., Ishigami, G., Hawthorne, S., Chen, H., Hansen, M., Telleria, M., Playter, R., and Iagnemma, K., "Design and Analysis of a Soft Mobile Robot Composed of Multiple Thermally Activated Joints Driven by a Single Actuator," IEEE International Conference of Robotics and Automation, 2010.

[6] Smith, Stuart A, *Flexures: Elements of Elastic Mechanisms*, USA: CRC Pres, 2000.

[7] http://objet.com/3D-Printer/Connex500/

[8] http://objet.com/Materials/Tango_Materials/

[9] http://www.cue-inc.com/technical-data-charts.html